

Influence of Antimony Doping on Structure and Morphology of ZnO Nanowires Grown by Vapor-Liquid-Solid Technique

M. Faisal Malik¹, M. Asghar^{1*}, M. A. Nawaz², F. Iqbal³, M. Y. Shahid³, M. Hashim¹, Mahdi-Al-Maghrabi⁴

1. Khwaja Farid University of Engineering and Information Technology, Rahim Yar Khan, Pakistan

2. Punjab College Chishtian, Pakistan

3. The Islamia University of Bahawalpur 6130, Pakistan

4. University of Yambo, Yambo, Kingdom of Saudi Arabia

* **Corresponding Author:** Email: asghar.hashmi@kfueit.edu.pk

Abstract

As-grown and antimony (Sb) doped ZnO nanowires (NWs) have been successfully grown on Au-coated Si(1 0 0) substrate by vapor-liquid-solid (VLS) method. The growth temperature was kept at 950°C purposefully to make Au layer act as a nucleation site. The length of Sb-doped ZnO NWs increases largely ~ 12 times longer than those of the undoped ZnO NWs; however, the earlier structure is thinner than the later. Scanning electron microscopy and X-ray diffraction measurement of Sb-ZnO wires present good NWs morphology and high purity and crystallinity of the samples, respectively. Similarly, the photoluminescence (PL) spectra of as-grown and Sb-doped ZnO NWs reveal the band-to-band transition without the significant defect level emission. However, PL peak due to the Sb-doped ZnO nanowires exhibits red shift as compared to that of as-grown ZnO NWs. Our results have been compared with the literature and interesting features have been discussed.

Keywords: Sb-doped ZnO Nanowires; Vapor-Liquid-Solid; SEM; X-ray Diffraction

1. Introduction

In recent years the interest in the growth of one-dimensional nanostructures like semiconductor nanowires is highly increased [1]. The nanostructure provides great potential in various fields e.g., nanophotonics, nano-electronics and bio-sensing. Semiconductor nanostructures, such as nanowires, nanorods, nanobelts and nanotubes have a great impact in industrial application especially in electronic, electromechanical and optoelectronic devices. Owing to their reduced size, one dimensional nanostructure possesses the improved electrical, electromechanical, optical, magnetic, and thermoelectric properties. The good control over the growth conditions is the key to effectively utilize the benefits offered by the nanostructure which ultimately will become the fundamental phenomenon in developing high performance devices [2]. The nanowires structures are continuously contributing towards the advancement of electronic and optical devices. The direct band gap (3.37eV) [3] and high exciton binding energy (60meV) of ZnO remain always the motivation to study the ZnO-based nanostructures. The interest in ZnO based nanostructure is further fuelled due to its broad application, including photo-detectors [4, 5], light-

emitting diodes [6, 7] field effect transistors [8, 9], piezoelectric transducers and solar cell [10,11]. Most of the applications of the nanostructure require the control over their geometry (diameter, length, etc.). In the case of ZnO nanowires it was highly desired to control the growth conditions which ultimately provide the good control over the morphology and shape of ZnO nanowires.

Owing to unique features and simplicity of fabrication, a plethora of research work has been published on the preparation, characterization, and applications of ZnO NWs. Different growth techniques like hydrothermal [12, 13], MOCVD [12, 14], MBE [15, 16], and VLS have been employed to grow the ZnO NWs. Among these techniques, the VLS has been used extensively for growing ZnO nanostructure on the metal-catalysed substrate. In case of Si substrate bare surface offers large mismatch in thermal expansion coefficient and lattice constant [17, 18]. Thus, metal coating is inevitable for the growth of large area and dense ZnO nanostructures. In the VLS process argon serves as the carrier gas and transports the Zn vapors to the Au droplet where the precipitation of the ZnO takes place until the saturation state is reached. Afterwards out of the melt, nucleation of the solid ZnO takes place

resulted in the formation of ZnO nanowires. The metal catalyst here provides the preferential site for the adsorption of the Zn vapors and will remain at the tip of the nanowires [19, 25].

The p-type doping in bulk ZnO is still a challenge because of electronic defects, which may be generated due to the difference of the lattice constant of p-type region from that of intrinsic region. These defects thus, counter the p-type doping effect from the intrinsic dopant [26]. However in the case of nanostructure, the single crystal growth reduces the lattice defects. Thus, the strain produced due to the incorporation of P-type dopant would not induce much defects with a limited dimension [26]. Various doping elements such as Na, N, P and Sb have been studied to increase the application possibility of ZnO nanostructures [11, 27, 29]. Yang et. al. [30] studied the incorporation of N in ZnO NWs and suggested that morphology is unaffected by N

doping, the reported length of as-grown ZnO nanowire is ~ 1-2µm and the diameter varies in the range of 80-130nm. Wu et. al. have fabricated Na-doped ZnO NWs by thermal decomposition route, according to their findings, Na doping has negligible effect on the size and morphology of the as-synthesized samples [31]. Lupan et. al. have grown the Ag and Sb doped ZnO nanorods with a facile hydrothermal technique, the length and diameter of the pure ZnO nanorods were 200µm and 200nm respectively which were not affected by Ag and Sb doping [32]. In summary, the effect of doping on the structure and morphology of the nanowires need more attention and can prove useful in controlling the dimensions of nanowires. Table 1 witnesses the effect of various dopants on the length and diameter of ZnO nanowires. The data indicates that information about the effect of Sb in ZnO lacks various features and hence requires further research.

Table 1: Growth method and effect of doping on Length and diameter of ZnO nanowires

Preparation method	Substrate	Doping	Length (µm)		Diameter (nm)		Temp °C	Ref
			As-grown	Doped	As-grown	Doped		
VLS	ZnO:Ga/Glass	Al	2.6	2.4	100	80-160	550	33
CVD	ZnO film on c-plane sapphire substrate	Sb	-	3.2	-	200	650	34
Aqueous Solution	Si with ZnO seed layer	Na	0.75	0.15	30	50	-	35
hydrothermal	Glass with ZnO seed layer	Ga	-	1.96	-	54	90	36
CVD	Si	In	-	10-15	-	70-311	550	37
CVD	sapphire	P	-	2	-	50-60	945	38
Wet- Chemical method	-	Fe	5	3	-	-	-	39
MOVPE	Al ₂ O ₃	-	3.5	-	150	-	800	-
VLS	ZnO	-	1-2	-	60-100	-	990	40
CVD	Si with ZnO seed layer	-	1.5-10	-	150	-	-	41
Thermal evaporation	Si	-	1.2	-	350-400	-	700	42
Thermal evaporation	sapphire	-	2.5	-	600-800	-	700	42
VLS	Si (100)	Sb	1.3	16	170	95	950	This study

In the case of ZnO nanowires, VLS growth with different catalysts has long been reported [43, 45]. In all these findings metal catalyst has been found on top of the ZnO nanowires. In this work, the growth of undoped and Sb-doped ZnO nanowires using the VLS method is investigated. We have discussed the structure and morphology of undoped and Sb-doped ZnO nanowires by X-ray diffraction analysis (XRD) and scanning electron microscopy (SEM). From the Williamson-Hall (W-H) procedure we gave information on the crystallite size and strain of undoped and Sb-doped ZnO nanowires. PL spectra of the undoped and Sb-doped samples have also suggested the important findings.

2. Experimental Procedure

ZnO NWs were grown on Au coated Si (1 0 0) substrate by VLS techniques. Thin film of Au ~ 8nm was deposited on substrate by thermal evaporation technique and thickness of film was controlled by thickness monitoring unit. Prior to growth, the substrates were cleaned in acetone, isopropanol and deionized water for 10 minutes each. The source used for the sample A was graphite and ZnO powder (99.99% pure of Alfa Aesar) mixed together by equal volume.

Alumina boat containing the source was transferred inside the quartz tube to the center of the furnace at a temperature of 1050 °C. The substrate was placed inside the quartz tube toward the lower temperature region of furnace. The argon flux was used to transfer the Zn vapors from the source to the substrate. The flow rate, and substrate temperature were varied to obtain 1-D growth of ZnO NWs and the best results were obtained for sample A at 950 °C with argon flux of 246 sccm. Other samples were grown at same temperature and argon flux, with addition of Sb powder along with ZnO and C powders. ZnO and C powder were mixed by equal volume with varying concentration of Sb powder, all mix together. Samples B, C, and D were having (ZnO + C): Sb = 30:1, 20:1 and 10:1 by volume,

respectively. The Sb as a dopant serves to control the dimensions of the ZnO nanowires.

3. Results and Discussion

The SEM image of Fig. 1 (top left) gives a general view of the as grown sample, where the nanowires simply present the VLS grown technique with Au tip at the end. The grown wires are dense and uniformly distributed which is generally the outcome of the metal coated Si substrate. We have randomly selected 10 nanowires from each sample and measured the dimension of nanowires by using the software Image J. Fig. 1 (top left) shows the SEM image of sample A and average length of the grown nanowires is approximately 1.3µm. The grown nanowires have the Au tip which is the evidence that growth mechanism involved is VLS. The process can be briefly explained as following: The Au droplet along with Zn form the eutectic alloy where Zn continues to absorb and the concentration of the Zn increases with time which supersaturates the Zn content in the alloy, afterwards the solid crystal nucleates out of the alloy droplet in the form of NWs with Au tip. In the growth of other samples, we have introduced the Sb powder in varying ratio in the reactants and observe the effect of Sb doping on the structure and morphology of the NWs. Incorporation of Sb into the ZnO nanowires plays a quite interesting role, the length of the wires increases to a manifold as compared to as-grown ZnO nanowires. Fig. 1 (top right), shows the dimensions of the nanowires of sample B having the length of 5µm and width of 127nm, the measured length is 4 times longer as compared to as-grown ZnO. Fig. 1 (lower left) shows the dimensions of nanowires of sample C having length of 8µm and width of 100nm, the measured length is 6 times longer than as-grown ZnO NWs. Fig. 1 (lower right) shows the dimensions of sample D having length of 16µm and width of 95nm, the measured length is almost 12 times longer as compared to as-grown ZnO listed in Table 2.



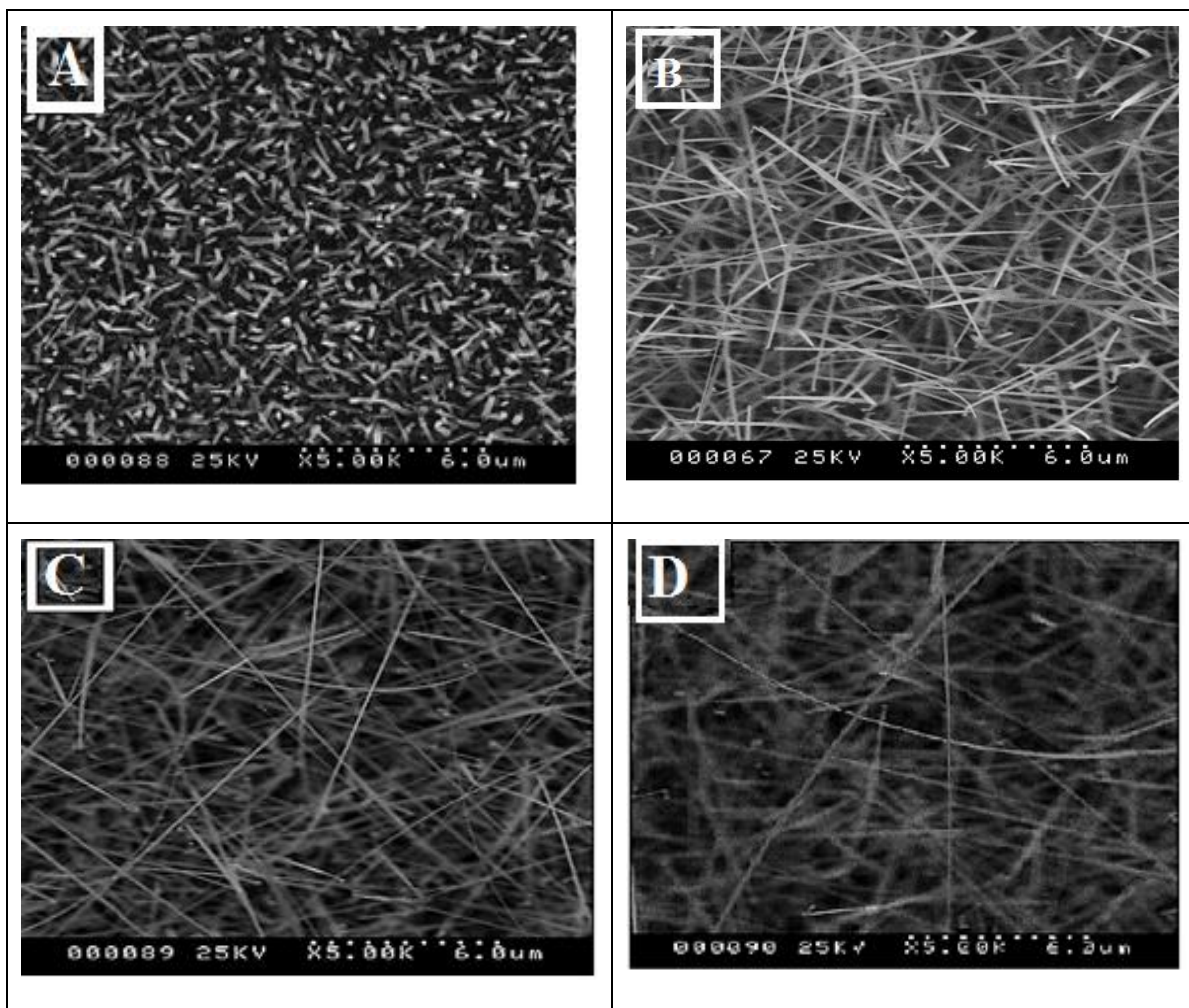


Fig. 1: SEM images: (top left) sample A, (top right) sample B, (lower left) sample C and (lower right) sample D grown by VLS process

The SEM images of samples B, C, and D present that Sb serves to grow the longer nanowires. The increase in length of wires takes place due to the following reasons (i) increase in the solubility of the Zn vapors (ii) decrease of Young Modulus [46] increases the strain in Sb doped ZnO nanowires, is responsible for the increase in length of the wires. The mathematical expression clearly explains the effect of Sb doping on the increase in length (ΔL) of ZnO nanowires.

$$Y = \frac{\text{Stress}}{\text{Strain}} = \frac{F \times L}{A \times \Delta L} \quad (4)$$

The Sb in the NWs increases the strain in the wires which results in the considerable increase in the length of nanowires. In other way, the same thickness of the Au film in all samples ensures the formation of Au droplet of same surface area, but the solubility of the Zn vapors increases with the increase of Sb concentration. The morphological changes due to the incorporation of Sb in ZnO NWs are illustrated in

Fig. 2, which shows that by increasing the Sb concentration in ZnO, the length of the nanowires increases while the diameter decreases.

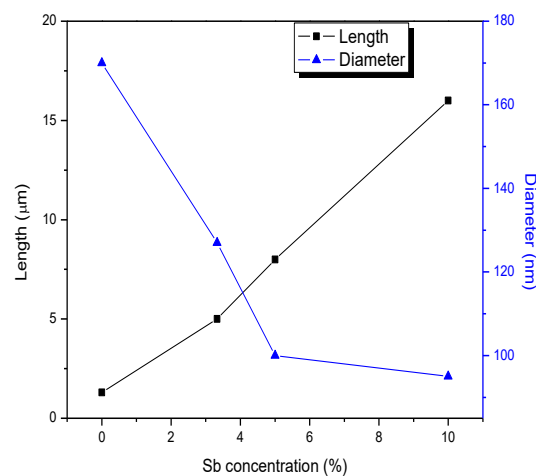


Fig. 2: Length and diameter of as-grown and Sb-doped ZnO NWs

Table 2: The growth mechanism of samples A, B, C and D

	Growth Temperature	Argon Flow	Source Used	Shape and Dimension of Nanostructure
Sample A	950 °C	246 sccm	ZnO and graphite equal by volume	ZnO NWs ~ 1.3µm width ~ 170nm
Sample B	950 °C	246 sccm	(ZnO+C):Sb = 30:1 by Volume	ZnO NWs of length ~ 5µm & width ~ 127nm
Sample C	950 °C	246 sccm	(ZnO+C):Sb = 20:1 by Volume	ZnO NWs of length ~ 8µm & width ~ 100nm
Sample D	950 °C	246 sccm	(ZnO+C):Sb = 10:1 by Volume	ZnO NWs of length ~ 16µm & width ~ 95nm

Fig. 3 shows the XRD patterns of samples A, B, C and D recorded in the range of 30° to 60° with the scanning step of 0.010°, the samples show the peaks which are ascribed to (1 0 0), (0 0 2), (1 0 1), (1 0 2) and (1 1 0) crystal planes of the hexagonal wurtzite structure of ZnO. All the

diffraction peaks are in good agreement with those of the standard JCPDS card (JCPDS No. 89-1397, and 89-0511). The diffraction peaks at 38.179° and 44.381° correspond to Au (1 1 1) and Sb (0 0 6), respectively.

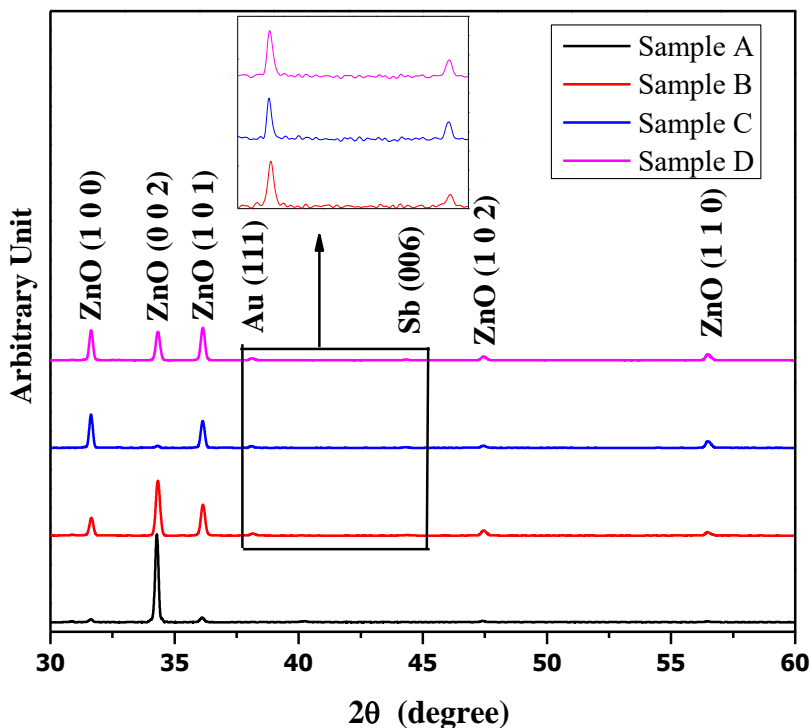


Fig. 3: XRD spectrum of samples A, B, C and D

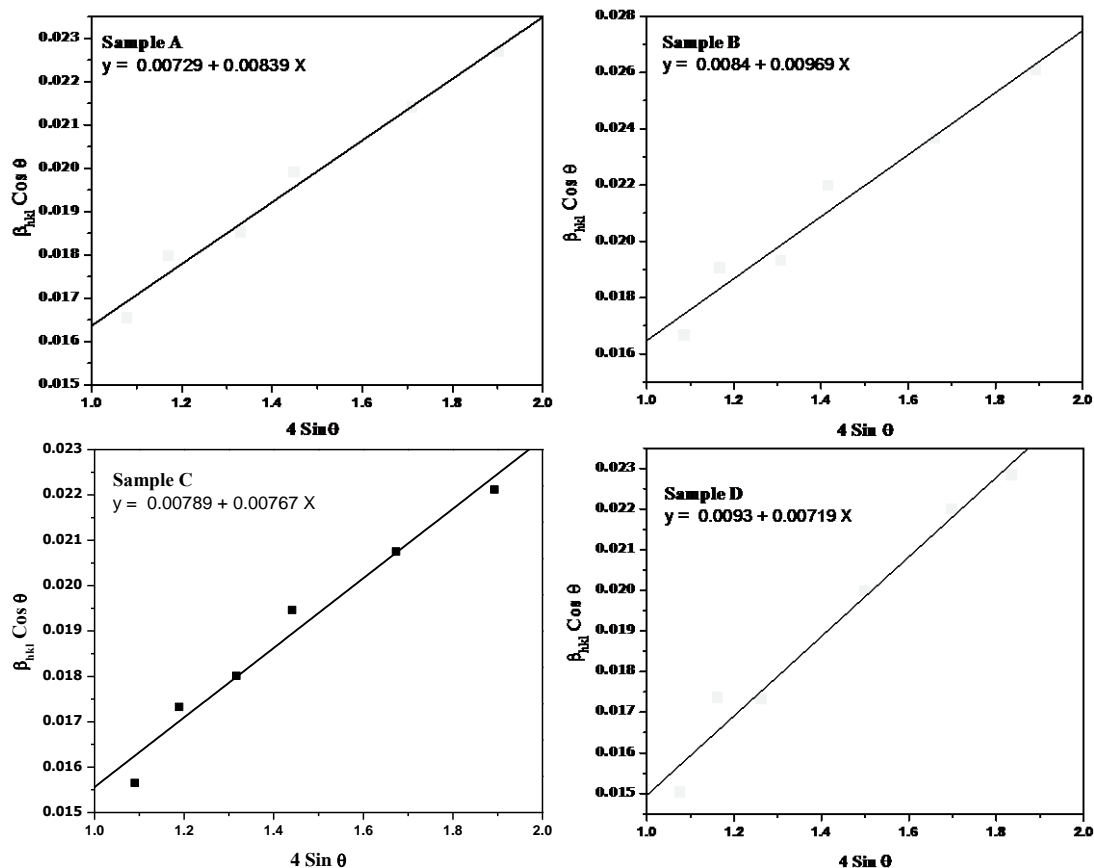


Fig. 4: W-H analysis of samples A, B, C and D by assuming UDM. Y-intercept and slope of the linear fit provided crystallite size D and microstrain ϵ , respectively

Various microstructural characteristics of ZnO are calculated and listed in Table 2. Lattice constants of ZnO are calculated by

$$a = b = \frac{\lambda}{\sqrt{3} \sin \theta} \quad \& \quad c = \frac{\lambda}{\sin \theta}$$

Different methods are reported to calculate crystallite size and strain but Uniform Deformation Model (UDM) of Williamson-Hall analysis is found to be more reliable [47]. By Scherrer formula

$$D = \frac{k\lambda}{\beta_t \cos \theta} \Rightarrow \beta_t = \frac{k\lambda}{D \cos \theta} \quad (5)$$

where D is the crystallite size, k is a constant ($k = 0.94$) and λ is the wavelength of incident X-rays ($\lambda = 0.15405 \text{ nm}$) and β_t is the full width half maximum. The strain-induced in ZnO samples due to dislocation along with imperfection of crystal was calculated by Wilson equation

$$\beta_s = 4\epsilon \tan \theta \quad (6)$$

where ϵ is the induced-strain, it is clearly seen from Eq. (4) and (5) that broadening of Bragg peak is the additive effect due to crystallite size and microstrain. Assuming the independently

effect of size and strain contribute the Bragg peak broadening and both have a Cauchy like profile, simply the observed broadening β_{hkl} is the sum of Eq. (4) and (5).

$$\beta_{hkl} = \beta_t + \beta_s \quad (7)$$

$$\beta_{hkl} = \left(\frac{k\lambda}{D \cos \theta} \right) + (4\epsilon \tan \theta) \quad (8)$$

Simplify Eq. (4)

$$\beta_{hkl} \cos \theta = \left(\frac{k\lambda}{D} \right) + (4\epsilon \sin \theta) \quad (9)$$

Above equation is called W-H equation. A plot of $4 \sin \theta$ along x-axis versus $\beta_{hkl} \cos \theta$ along y-axis is drawn as shown in Fig. 4. UDM based on the assumption that strain is uniformly distributed in all direction of crystal; the isotropic nature of crystal is considered where all properties of material are independent of the direction along which they were measured [48]. The UDM analysis of ZnO is shown in Fig. 4. After linear fit of the data, y-intercepts and slope of the linear fit provided crystallite size D and microstrain ϵ are listed in Table 3 which reveals that by increasing the Sb concentration the crystallinity of ZnO NWs are actually improved which support SEM results.

Table 3: Lattice constants, crystalite size and microstrain of samples A, B, C and D

0.	$a = b$ (nm)	c (nm)	Crystalite Size (nm)	Microstrain
Sample A	0.326	0.522	88	8.18×10^{-3}
Sample B	0.326	0.522	91	9.69×10^{-3}
Sample C	0.326	0.521	93	7.67×10^{-3}
Sample D	0.326	0.522	98	7.19×10^{-3}

PL properties of as-grown and Sb-doped ZnO under the excitation wavelength of 247nm have been studied. Fig. 5 shows the PL spectrum for all the samples, the emission peaks for samples A, B, C and D are observed at 3.50eV, 3.46eV, 3.40eV, and 3.40eV respectively. These samples are showing the high value of emission energy especially sample A has shown the peak emission at 3.50eV. In Fig. 5, the red shift of the peak was observed for the Sb-doped ZnO sample as compared to as-grown ZnO sample. This red shift may be due to the nanostructure formation by incorporation of Sb into ZnO. It is also revealed that incorporation of Sb into the NWs causes the band tailing which is responsible for the peak broadening in the PL spectrum [49]. The study of ZnO NWs properties by PL may lead to the important applications in the future nano-photonics, nano-electronics and nano-optoelectronics.

4. Conclusion

We have studied the growth of undoped and Sb-doped ZnO nanowires on Au coated Si substrate by a VLS method. The average length of the undoped nanowires is $\sim 1.3\mu\text{m}$. Our results showed that by increasing the concentration of Sb in the alloy, the length of Sb-doped ZnO nanowires increases subsequently. Further, we have discussed the role of Sb in achieving the growth of longer 1-D ZnO nanowires. Sb serves to increase the Zn supply in Au-Zn alloy. Thus, incorporation of Sb alters the structure and morphology of the Sb-doped ZnO nanowires. XRD, and W-H analysis have shown that Sb-doped ZnO nanowires have good crystallinity. PL spectrum of the Sb-doped ZnO nanowires has shown red shift with the peak broadening.

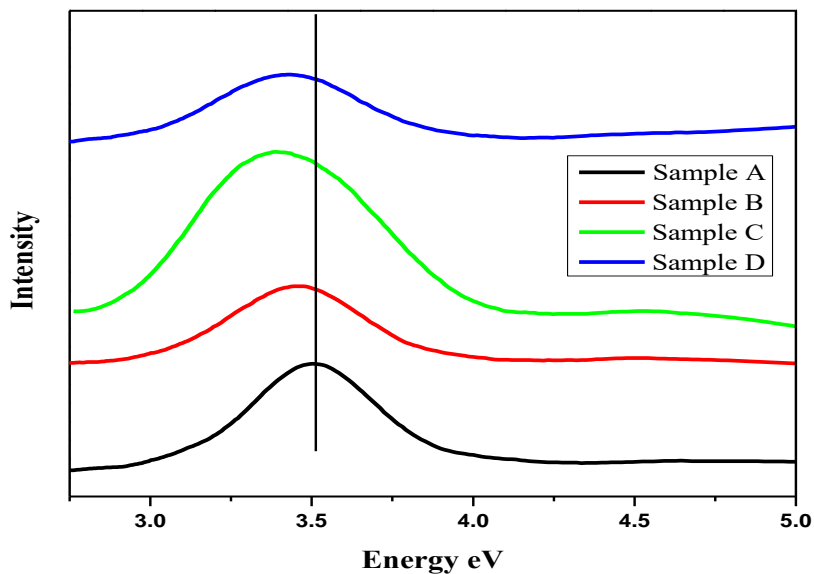


Fig. 5: PL Spectrum of Sample A, B, C and D

5. ACKNOWLEDGMENTS

The author M. Asghar is thankful to Higher Education Commission (HEC) of Pakistan to present this research in ICDS 2017, Matsue Japan.

6. REFERENCES

- [1] Kitazawa, N., Aono, M., and Watanabe, M. (2014), Growth of vertically aligned one-dimensional ZnO nanowire arrays on sol-gel derived ZnO thin films, *J. Phys. Chem. Sol.* 75, 1194-1200
- [2] Lieber, C., & Wang, Z. (2007). Functional Nanowires. *MRS Bulletin*, 32(02), 99-108.
- [3] Zhu, Y., Yang, H., Sun, F., & Wang, X. (2016). Controllable Growth of Ultrathin P-doped ZnO Nanosheets. *Nanoscale Research Letters*, 11(1), 175.
- [4] Ridhuan, N., Lockman, Z., Aziz, A., & Khairunisak, A. (2011). Properties of ZnO Nanorods Arrays Growth via Low Temperature Hydrothermal Reaction. *Advanced Materials Research*, 365, 422-426
- [5] Hassan N. K., Hashim M. R., Mahdi M. A., and Allam N. K. (2012), A catalyst-free growth of ZnO nanowires, *ECS J. Soli. Stat. Sci. Technol.* 1, 86-89.
- [6] Sun, J., Bian, J., Wang, Y., Wang, Y., Gong, Y., & Li, Y. et al. (2012). Fabrication of a Homo Junction Light Emitting Diode with ZnO-Nanorods /ZnO: As-Film Structure. *Electrochemical And Solid-State Letters*, 15, H164-H166.
- [7] Abbasi, M., Ibutoto, Z., Hussain, M., Nur, O., & Willander, M. (2013). The fabrication of white light-emitting diodes using the n-ZnO/NiO/p-GaN heterojunction with enhanced luminescence. *Nanoscale Research Letters*, 8(1), 320.
- [8] Hong, W., Sohn, J., Hwang, D., Kwon, S., Jo, G., & Song, S. et al. (2008). Tunable Electronic Transport Characteristics of Surface-Architecture-Controlled ZnO Nanowire Field Effect Transistors. *Nano Letters*, 8(3), 950-956.
- [9] Feng, Y., Lee, K., Farhat, H., & Kong, J. (2009). Current on/off ratio enhancement of field effect transistors with bundled carbon nanotubes. *Journal Of Applied Physics*, 106 (10), 104505.
- [10] Cai, F., Wang, J., Yuan, Z., & Duan, Y. (2012). Magnetic-field effect on dye-sensitized ZnO nanorods-based solar cells. *Journal Of Power Sources*, 216, 269-272.
- [11] Hussain, S., Khan, Y., Khranovskyy, V., Muhammad, R., & Yakimova, R. (2013). Effect of oxygen content on the structural and optical properties of ZnO films grown by atmospheric pressure MOCVD. *Progress In Natural Science: Materials International*, 23(1), 44-50
- [12] Rivera, A., Zeller, J., Sood, A., & Anwar, M. (2013). A Composition of ZnO Nanowires and Nanorods Grown Using MOCVD and Hydrothermal Processes. *Journal Of Electronic Material*, 42(5), 894-900.
- [13] Chen, W., Wu, J., Lin, J., Lo, S., Lin, H., & Hang, D. et al. (2013). Room-temperature violet luminescence and ultraviolet photodetection of Sb-doped ZnO/Al-doped ZnO homo junction array. *Nanoscale Research Letters*, 8(1), 313.
- [14] Black, K., Chalker, P., Jones, A., King, P., Roberts, J., & Heys, P. (2010). A New Method for the Growth of Zinc Oxide Nanowires by MOCVD using Oxygen-Donor Adducts of Dimethylzinc. *Chemical Vapor Deposition*, 16(1-3), 106-111.
- [15] Isakov, I., Panfilova, M., Sourribes, M., & Warburton, P. (2013). Growth of ZnO and ZnMgO nanowires by Au-catalysed molecular-beam epitaxy. *Physica Status Solidi (C)*, n/a-n/a.
- [16] Wei, W., Gao, J., Jiang, Z., Lü, X., & Xie, J. (2015). Transforming MoO₃ macrorods into bismuth molybdate nanoplates via the surfactant-assisted hydrothermal method. *Ceramics International*, 41(9), 11471-11481.
- [17] Pung, S., Tee, C., Choy, K., & Hou, X. (2012). Growth Mechanism of Au-Catalyzed ZnO Nanowires: VLS or VS-VLS?. *Advanced Materials Research*, 364, 333-337.
- [18] Hsu, H., Cheng, C., Chang, C., Yang, S., Chang, C., & Hsieh, W. (2005). Orientation-enhanced growth and optical properties of ZnO nanowires grown on porous silicon substrates. *Nanotechnology*, 16(2), 297-301.
- [19] Brewster, M., Zhou, X., Lim, S., & Gradečak, S. (2011). Role of Au in the Growth and Nanoscale Optical Properties of

- ZnO Nanowires. *The Journal Of Physical Chemistry Letters*, 2(6), 586-591.
- [20] Kar, A., Low, K., Oye, M., Stroschio, M., Dutta, M., Nicholls, A., & Meyyappan, M. (2011). Investigation of Nucleation Mechanism and Tapering Observed in ZnO Nanowire Growth by Carbothermal Reduction Technique. *Nanoscale Research Letters*, 6, 1-9
- [21] Saunders, R., Garry, S., Byrne, D., Henry, M., & McGlynn, E. (2012). Length versus Radius Relationship for ZnO Nanowires Grown via Vapor Phase Transport. *Crystal Growth & Design*, 12(12), 5972-5979.
- [22] Ramgir, N., Subannajui, K., Yang, Y., Grimm, R., Michiels, R., & Zacharias, M. (2010). Reactive VLS and the Reversible Switching between VS and VLS Growth Modes for ZnO Nanowire Growth. *The Journal Of Physical Chemistry C*, 114(23), 10323-10329.
- [23] Zhu, Y., Yang, H., Sun, F., & Wang, X. (2016). Controllable Growth of Ultrathin P-doped ZnO Nanosheets. *Nanoscale Research Letters*, 11(1), 175.
- [24] Pung, S.Y., Tee, C.C., Choy, K.L. and Hou, X.H., 2012. Growth Mechanism of Au-Catalyzed ZnO Nanowires: VLS or VS-VLS?. In *Advanced Materials Research*, 364, 333-337).
- [25] Hsu, H.C., Cheng, C.S., Chang, C.C., Yang, S., Chang, C.S. and Hsieh, W.F., 2005. Orientation-enhanced growth and optical properties of ZnO nanowires grown on porous silicon substrate. *Nanotechnology*, 16, 297.
- [26] Sun, X., & Yang, Y. (2016). *ZnO nanostructures and their applications*. Pan Stanford.
- [27] Bu, I. (2016). Sol-gel production of p-type ZnO thin film by using sodium doping. *Superlattices and Microstructures*, 96,59-66.
- [28] Pathak, T., Kumar, V., & Purohit, L. (2015). High quality nitrogen-doped zinc oxide thin films grown on ITO by sol-gel method. *Physica E: Low-Dimensional Systems and Nanostructures*, 74, 551-555.
- [29] Xiu, F., Yang, Z., Mandalapu, L., Zhao, D., Liu, J., & Beyermann, W. (2005). High-mobility Sb-doped p-type ZnO by molecular-beam epitaxy. *Applied Physics Letters*, 87(15), 152101.
- [30] Yang, X., Wolcott, A., Wang, G., Sobo, A., Fitzmorris, R., & Qian, F. et al. (2009). Nitrogen-Doped ZnO Nanowire Arrays for Photoelectrochemical Water Splitting. *Nano Letters*, 9(6), 2331-2336.
- [31] Wu, C., & Huang, Q. (2010). Synthesis of Na-doped ZnO nanowires and their photocatalytic properties. *Journal Of Luminescence*, 130(11), 2136-2141.
- [32] Lupan, O., Chow, L., Ono, L., Cuenya, B., Chai, G., & Khallaf, H. et. al. (2010). Synthesis and Characterization of Ag- or Sb-Doped ZnO Nanorods by a Facile Hydrothermal Route. *The Journal Of Physical Chemistry C*, 114(29), 12401-12408.
- [33] Hsu, C., Chang, S., Hung, H., Lin, Y., Huang, C., Tseng, Y., & Chen, I. (2005). Well-Aligned, Vertically Al-Doped ZnO Nanowires Synthesized on ZnO:Ga/Glass Templates. *Journal Of The Electrochemical Society*, 152, 378-381.
- [34] Chu, S., Wang, G., Zhou, W., Lin, Y., Chernyak, L., & Zhao, J. et al. (2011). Electrically pumped waveguide lasing from ZnO nanowires. *Nature Nanotechnology*, 6, 506.
- [35] Yin, J., Yang, C., Yang, X., Wang, S., Zhang, H., Zhou, S., & Feng, G. (2016). Fabrication and Photocatalytic Properties of ZnSe Nanorod Films. *Journal Of Nanomaterials*, 2016.
- [36] Young, S., Chiou, C., Liu, Y., & Ji, L. (2016). Synthesis of Ga-Doped ZnO Nanorods by Hydrothermal Method and their Application to Ultraviolet Photodetector. *Inventions*, 1, 3.
- [37] Lim, S., Brahma, S., Liu, C., Wang, R., & Huang, J. (2013). Effect of indium concentration on luminescence and electrical properties of indium doped ZnO nanowires. *Thin Solid Films*, 549, 165-171.
- [38] Xiang, B., Wang, P., Zhang, X., Dayeh, S., Aplin, D., & Soci, C. et al. (2007). Rational Synthesis of p-Type Zinc Oxide Nanowire Arrays Using Simple Chemical Vapor Deposition. *Nano Letters*, 7(2), 323-328.
- [39] Iqbal, J., Jan, T., Ronghai, Y., Naqvi, S., & Ahmad, I. (2014). Doping Induced Tailoring in the Morphology, Band-Gap and

- Ferromagnetic Properties of Biocompatible ZnO Nanowires, Nanorods and Nanoparticles. *Nano-Micro Letters*, 6, 242-251.
- [40] Sallet, V., Sartel, C., Vilar, C., Lusson, A., & Galtier, P. (2013). Opposite crystal polarities observed in spontaneous and vapour-liquid-solid grown ZnO nanowires. *Applied Physics Letters*, 102(18).
- [41] Protasova, L., Rebrov, E., Choy, K., Pung, S., Engels, V., & Cabaj, M. et. al. (2011). ZnO based nanowires grown by chemical vapour deposition for selective hydrogenation of acetylene alcohols. *Catalysis Science & Technology*, 1, 768-777.
- [42] Srivatsa, K., Chhikara, D., & Kumar, M. (2011). Synthesis of Aligned ZnO Nanorod Array on Silicon and Sapphire Substrates by Thermal Evaporation Technique. *Journal Of Materials Science & Technology*, 27(8), 701-706.
- [43] Yang, P., Yan, H., Mao, S., Russo, R., Johnson, J., & Saykally, R. et. al. (2002). Controlled Growth of ZnO Nanowires and Their Optical Properties. *Advanced Functional Materials*, 12(5), 323-331.
- [44] Wang, X., Summers, C., & Wang, Z. (2004). Large-Scale Hexagonal-Patterned Growth of Aligned ZnO Nanorods for Nano-optoelectronics and Nanosensor Arrays. *Nano Letters*, 4(3), 423-426.
- [45] Gao, P., Ding, Y., & Wang, Z. (2003). Crystallographic Orientation-Aligned ZnO Nanorods Grown by a Tin Catalyst. *Nano Letters*, 3(9), 1315-1320.
- [46] Yang, Y., Qi, J., Guo, W., Liao, Q., & Zhang, Y. (2010). Mechanical and longitudinal electromechanical properties of Sb-doped ZnO nanobelts. *Crystengcomm*, 12(7), 2005-2007.
- [47] Nawaz, M.A., Asghar, M., Shahid, M.Y., UL, A., Iqbal, F., Malik, F. and Ruda, H.E., 2016. Microstructural Study of as-Grown and 650°C Annealed ZnO Nanorods: X-ray Peak Profile Analysis. *Digest J. Nanomaterials and Biostructures*, 11, 537-546.
- [48] Asghar, M., Shahid, M., Iqbal, F., Fatima, K., Nawaz, M., Arbi, H., & Tsu, R. (2016). Simple method for the growth of 4H silicon carbide on silicon substrate. *AIP Advances*, 6(3).
- [49] Li, Q., Cheng, K., Weng, W., Du, P., & Han, G. (2013). Synthesis, characterization and electrochemical behavior of Sb-doped ZnO microsphere film. *Thin Solid Films*, 544, 466-471.